J Eng Math (2009) 65:291–310
DOI 10.1007/s10665-009-9314-y

Electrically induced bubble deformation, translation and collapse

S. J. Shaw · P. D. M. Spelt · O. K. Matar

Received: 16 July 2007 / Accepted: 9 July 2009 / Published online: 29 July 2009

Abstract In this work, the behaviour of a gas bubble in a low-Mach-number, weakly viscous, dielectric liquid under the action of a spatially uniform electric field is considered. Using domain perturbation analysis and assuming any shape deformation of the bubble or induced translation to be small, but placing no such restriction on the volume oscillations, appropriate equations to second order in the small-interaction terms are derived. Steady and time-dependent solutions are presented. The results indicate that only even shape modes and odd components of the interfacial charge density are excited starting from an initially stationary and uncharged spherical bubble. In order for the bubble to be set into motion it must either be initially deformed in terms of an odd shape mode or acquire an even charge density component. Situations are examined wherein all modes are excited and the presence of an instability that arises due to a coupling between an even mode of the charge density and bubble translation is demonstrated. The instability manifests itself via the sudden acceleration of the bubble and growth of its radius; this leads ultimately to conditions beyond the reach of the present theory.

Keywords Bubble dynamics · Electric field · Fluid mechanics · Sonoluminescence

1 Introduction

Electric fields can be used to control the dynamics of bubbles such that a variety of processes can be improved. These include nucleate boiling, wherein application of an electric field causes bubbles to translate or to break up, leading to enhanced boiling heat transfer (e.g., [1]), and the growth and detachment of bubbles at an orifice [2]. In the context of sonoluminescence, Spelt and Matar [3] showed theoretically that more violent collapse could be achieved by subjecting freely suspended bubbles to an electric field, which would naturally also be of interest in other areas such as electrochemistry, ultrasonic imaging, drug delivery, surface cleaning, sonochemistry and in both nuclear and marine technologies. A complication, however, is that this improved collapse is accompanied by a growth of the ellipsoidal shape mode of the bubble, which becomes more pronounced as minimum volume is approached. Clearly, this concurrent increase in shape deformation (which would also be expected to trigger other shape modes) could have a detrimental impact on the bubble collapse, and hence the determination of favourable conditions under which the use of electric fields could enhance sonoluminescence.

S. J. Shaw (✉) · P. D. M. Spelt · O. K. Matar
Department of Chemical Engineering, Imperial College London, South Kensington Campus, London SW7 2AZ, UK
e-mail: s.shaw@imperial.ac.uk

Previous theoretical studies on the dynamics of a bubble in an electric field have utilized either an approach that is fully linear in volume and shape deviations (e.g., [4], where the degree to which the natural frequency values of shape modes are modified by electric fields is determined), or an approach that accounts for shape modes only in a linear manner but that allows for bubbles to collapse violently; Oh et al. [5], for instance, investigated the occurrence of chaotic volume and shape oscillations; see further the study by Spelt and Matar [3] discussed above. In the two latter studies, for the case of a spatially uniform electric field, only the effect on the volume and a single shape mode was accounted for. Approaches that allow for nonlinear coupling between shape modes have been developed extensively for droplets in an electric field (see for example [6–18]), but appear not yet to have been applied directly to bubbles, and it remains unclear which and how bubble shape modes interact in an electric field. To our knowledge, an analysis that is nonlinear in shape-mode amplitudes and allows for the collapse of a bubble has also not been attempted previously.

An important difference between drops and bubbles is that in the latter case volume conservation is not imposed. Indeed, the contents of the bubble are assumed to be compressible. This impacts not only on the volume oscillations of the bubble but also both the translation and shape deformation through nonlinear interaction. A second difference is that the gaseous contents of the bubble have a much smaller permittivity than the content of drops—the dielectric constant for water at room temperature is 80 times larger than the corresponding value for air. In turn this causes a liquid drop to undergo more elongation in an electric field than a gas bubble for the same strength of electric field (see, for example, [19]).

In light of the above observations we derive here a theoretical model of the dynamics of a bubble in an electric field, allowing for violent collapse, translation and shape deformations. Firstly, we represent any shape deformation by an infinite sum of Legendre polynomials, obtaining suitable evolution equations for the amplitudes of the respective Legendre polynomials through the application of perturbation analysis with respect to the bubble surface boundary conditions. The analysis is conducted to second order in the small shape-mode amplitudes. We determine clearly the conditions under which the higher modes become excited. The resulting model is a system of nonlinear, coupled ordinary differential equations that can be integrated numerically in an efficient manner for a large range of cases. In principle, the model can be extended to model the detailed dynamics of several bubbles in an electric field, but this is beyond the scope of this paper. We conclude the paper by demonstrating the impact of the shape and charge density modes on the collapse, translation and deformation of the bubble.

2 Problem formulation

2.1 Governing equations

A gas bubble of relative permittivity $\overline{\varepsilon}_{\text{in}}$ and conductivity κ_{in} is subjected to a spatially uniform electric field $\mathbf{E}_0$ (its value may depend on time, but this notation is suppressed here) in a liquid of relative permittivity $\overline{\varepsilon}$ and conductivity κ; the subscript 'in' is used to designate quantities associated with the bubble contents. The electric fields, $\mathbf{E}$ and $\mathbf{E}_{\text{in}}$, are assumed to be irrotational and solenoidal, thus $(\mathbf{E}, \mathbf{E}_{\text{in}}) = (\nabla\psi(\mathbf{x}, t), \nabla\psi_{\text{in}}(\mathbf{x}, t))$ and satisfy the following equations

$$\nabla^2\psi = 0 \quad \text{and} \quad \nabla^2\psi_{\text{in}} = 0, \tag{1}$$

where ψ, ψ_{in} denote the respective electric potentials; the position vector $\mathbf{x}$ is measured relative to the bubble centre, t represents time and S corresponds to the interface between the gas and liquid phases.

The electrostatic interfacial boundary conditions are the continuity of the tangential component of the electric field displacement vector, the jump condition for the normal component of the electric field displacement vector and the unsteady balance of free charge at the interface which are given respectively by [3,20]

$$\psi = \psi_{\text{in}} \quad \text{on } S, \tag{2}$$

$$\left[\overline{\varepsilon}\hat{\mathbf{n}} \cdot \nabla\psi - \overline{\varepsilon}_{\text{in}}\hat{\mathbf{n}} \cdot \nabla\psi_{\text{in}}\right]_S = q/\overline{\varepsilon}_0, \tag{3}$$

$$\left[-\kappa\hat{\mathbf{n}}\cdot\nabla\psi+\kappa_{\text{in}}\hat{\mathbf{n}}\cdot\nabla\psi_{\text{in}}\right]_S=\frac{\mathrm{d}q}{\mathrm{d}t}+\nabla_S\cdot(q\mathbf{u}),\tag{4}$$

where $\hat{\mathbf{n}}$ is the unit normal vector at the bubble surface pointing into the liquid, q is the interfacial charge density and $\mathbf{u}$ the liquid velocity; $\overline{\varepsilon}_0$ and $\overline{\varepsilon}$ are the permittivity of free space and the dielectric constant of the liquid phase. The surface gradient operator $\nabla_S=\nabla-\hat{\mathbf{n}}(\hat{\mathbf{n}}\cdot\nabla)$, while we define the velocity in the normal direction as $\mathbf{u}_n=\hat{\mathbf{n}}(\hat{\mathbf{n}}\cdot\mathbf{u})$. Since

$$\nabla_S\cdot(q\mathbf{u})=\nabla_S\cdot(q\mathbf{u}_\mathbf{S})+q(\nabla_S\cdot\hat{\mathbf{n}})(\mathbf{u}\cdot\hat{\mathbf{n}})=\nabla_S\cdot(q\mathbf{u}_\mathbf{S})+q(\nabla\cdot\hat{\mathbf{n}})(\mathbf{u}\cdot\hat{\mathbf{n}}),\tag{5}$$

where $\mathbf{u}_\mathbf{S}=\mathbf{u}-\mathbf{u}_n$, these terms are exactly those presented by Belonozhko and Grigor'ev [21]. It is also straightforward to show that these terms are consistent with the pertinent terms presented by Saville [20].

Close scrutiny of the analysis in [20–22] reveals that they all are in a frame of reference moving with velocity $\mathbf{u}_n$, i.e., moving in a frame of reference with the interface. This is not so in our work. We define our problem relative to a frame of reference moving with the velocity of the bubble, redefining the velocity field accordingly. A further modification to the interfacial charge-density boundary condition is required, however. Although the charge density q is only defined at the interface, as we Fourier decompose it (this will be done below), the resultant expression is an analytical continuation in the radial direction with $\partial q/\partial r=0$. Therefore, the time derivative in (4) is evaluated as follows [23,24]

$$\frac{\mathrm{d}q}{\mathrm{d}t}=\frac{\partial q}{\partial t}+\mathbf{u}_n\cdot\nabla q=\frac{\partial q}{\partial t}+\mathbf{u}_n\cdot\hat{\mathbf{e}}_\theta\frac{\partial q}{\partial\theta},\tag{6}$$

where $\hat{\mathbf{e}}_\theta$ is the unit normal vector in the θ-direction. As a result, Eq. 4 becomes

$$\frac{\partial q}{\partial t}+\mathbf{u}_n\cdot\hat{\mathbf{e}}_\theta\frac{\partial q}{\partial\theta}+\nabla_S\cdot(q\mathbf{u}_\mathbf{S})+q(\nabla\cdot\hat{\mathbf{n}})(\mathbf{u}\cdot\hat{\mathbf{n}})=\left[-\kappa\hat{\mathbf{n}}\cdot\nabla\psi+\kappa_{\text{in}}\hat{\mathbf{n}}\cdot\nabla\psi_{\text{in}}\right]_S.\tag{7}$$

We also impose the kinematic boundary condition at the bubble surface,

$$\frac{\mathrm{D}S}{\mathrm{D}t}=\frac{\partial S}{\partial t}+\mathbf{u}\cdot\nabla S=0,\tag{8}$$

as well as the following conditions on the normal and tangential components of the total stress, respectively:

$$\left[\hat{\mathbf{n}}\cdot\mathbf{T}\cdot\hat{\mathbf{n}}\right]_{S^-}^{S^+}=\sigma\nabla\cdot\hat{\mathbf{n}},\tag{9}$$

$$\left[\hat{\mathbf{n}}\cdot\mathbf{T}\cdot\hat{\mathbf{t}}\right]_{S^-}^{S^+}=0,\tag{10}$$

where σ is the surface tension, $\hat{\mathbf{t}}$ is the unit tangent vector at the bubble surface, $\mathbf{T}$ is the total stress tensor given by

$$\mathbf{T}=\mathbf{T}^f+\mathbf{M},\tag{11}$$

in which $\mathbf{T}^f$ and $\mathbf{M}$ correspond to the stress in the fluid phases and the Maxwell stress tensor, respectively, where

$$\mathbf{M}=\overline{\varepsilon}\,\overline{\varepsilon}_0\left(\mathbf{EE}-\frac{1}{2}E^2\mathbf{I}\right);\tag{12}$$

here, $\mathbf{I}$ is the identity tensor. The viscous contribution to the tangential stress condition (10), which is important for charged droplets, is ignored here. Hence we assume the flow in the liquid phase to be irrotational so that the liquid velocity is given by $\mathbf{u}=\nabla\phi$ where ϕ is a potential function; we account for viscous corrections by employing a boundary-layer approach as discussed further below.

2.2 Domain perturbations

We use a spherical polar coordinate system (r,θ,Ψ) relative to the bubble centre to model the bubble dynamics. Restricting attention to small, axisymmetric deformation, we may give the bubble surface S by

$$S(r,\mu,t)=r-R(t)-\epsilon\sum_{k=2}^{\infty}a_k(t)P_k(\mu)=0,\tag{13}$$

where $R(t)$ represents the spherical oscillations of the bubble, $\mu = \cos\theta$ and $P_k(\mu)$ is a Legendre polynomial of degree k, with corresponding scaled amplitude $a_k(t)$. The amplitudes have been scaled by a small dimensionless parameter ϵ (a representative value of the maximum ratio of the shape amplitudes and R) in order to facilitate the subsequent presentation; an exact definition of ϵ is not needed, the final model equations are in terms of ϵa_k. Suitable evolution equations for the volume oscillations $R(t)$ and shape-mode amplitudes $\epsilon a_k(t)$, $k \in [2, \infty)$, are obtained by applying perturbation analysis with respect to the bubble-surface boundary conditions. We employ domain perturbation analysis obtaining corrections to $O(\epsilon^2)$ in a manner similar to the pertubation work of Doinikov [25]. We note that many perturbation studies with respect to nonlinear bubble dynamics use multiple-scale analysis where the shape-mode amplitudes are assumed to scale as $\epsilon^n a_n(t)$, $n \in [2, \infty)$. Here we wish to determine all permissible interactions of the form $a_i(t)a_j(t)$, $i, j \in [2, \infty)$, in order to determine how energy is transferred between the shape modes when a bubble is being forced by an electric field.

Following Spelt and Matar [3], the electric potentials both inside the bubble and in the liquid are also assumed to be axisymmetric having the form

$$\psi(r, \mu, t) = \left(E_0 + \frac{A(t)R(t)^3}{r^3}\right) r P_1(\mu) + \epsilon \sum_{k=2}^{\infty} \frac{A_k(t)}{r^{k+1}} P_k(\mu), \tag{14}$$

$$\psi_{\text{in}}(r, \mu, t) = B(t) r P_1(\mu) + \epsilon \sum_{k=2}^{\infty} B_k(t) r^k P_k(\mu). \tag{15}$$

Here E_0 is the magnitude of the applied electric field, while the coefficients $A(t)$, $A_k(t)$, $B(t)$, $B_k(t)$ ($k \in [2, \infty)$) are determined by applying the electrostatic interfacial boundary conditions, given by Eqs. 2 and 3. The interfacial charge density is given by

$$q(\mu, t) = \hat{q}(t) P_1(\mu) + \epsilon \sum_{k=2}^{\infty} \hat{q}_k(t) P_k(\mu), \tag{16}$$

where the coefficients $\hat{q}(t)$ and $\hat{q}_k(t)$ are again determined from the bubble-surface boundary conditions.

At low Mach numbers, the liquid velocity potential is [3,26,27]

$$\phi(r, \mu, t) = G(t) + \frac{D_0(t)}{r} + \epsilon \sum_{k=1}^{\infty} \frac{D_k(t)}{r^{k+1}} P_k(\mu), \tag{17}$$

where $G(t) = \phi_\infty + \frac{\rho}{c_\infty} \frac{\mathrm{d}}{\mathrm{d}t}(R^2 \dot{R})$, in which ϕ_∞ is the liquid velocity potential and c_∞ is the speed of sound in the liquid in the absence of the bubble, and ρ the density of the liquid. The overdot notation indicates differentiation with respect to time. Note that a term has been added to (17), i.e., the $k = 1$ case, relative to the equation presented by Spelt and Matar [3] in order to account for situations involving bubble translation. The addition of low-Mach-number compressibility effects to the model permits the more accurate study of violent bubble collapse. As the motion of the bubble wall increases significantly, due to compressibility effects, some of the energy associated with the volume oscillations is converted into acoustic emissions. This is most likely to occur around the bubble minimum volume. Accounting for this damping mechanism results in a reduction in the amplitude of the volume oscillations together with an increase in their frequency. In turn, through nonlinear interaction, this will modify all the other modes. Observable differences in the volume oscillations, though, are only seen for very violent collapse; see, for example, Fig. 6.

The coefficients $D_k(t)$, $k \in [0, \infty)$ are determined by applying the kinematic boundary condition.

In terms of a spherical polar coordinate system whose origin is at the bubble centre, the kinematic boundary condition at S, Eq. 8, has the form

$$\frac{\mathrm{D}S}{\mathrm{D}t} = \frac{\partial S}{\partial t} - \epsilon u_3(t)(\cos\theta, -\sin\theta, 0) \cdot \nabla S + \nabla\phi \cdot \nabla S = 0, \tag{18}$$

where we have assumed the bubble to be moving with speed $\epsilon u_3(t)$ along the axis of symmetry of the problem, which is taken to lie along the $\mathbf{z}$-axis in a stationary Cartesian coordinate system. We omit the resultant expressions

for the $D_k(t)$ coefficients (which may be found in the work of Doinikov [25]). Also, to aid presentation, we now omit explicit dependence on t.

We turn our attention now to the normal-stress balance at the interface. Substitution of the appropriate expression for $\mathbf{T}^f$ in (9) yields

$$p_g = -\rho\frac{\partial\phi}{\partial t} + \rho\epsilon u_3\,(\cos\theta, -\sin\theta, 0)\cdot\nabla\phi - \frac{1}{2}\rho\,|\nabla\phi|^2 + \sigma\nabla\cdot\hat{\mathbf{n}} + \Lambda - \left[\hat{\mathbf{n}}\cdot\mathbf{M}\cdot\hat{\mathbf{n}}\right]_{S^-}^{S^+}, \tag{19}$$

where p_g is the pressure of the gas within the bubble and Λ represents the viscous contributions. In order to account for the viscous damping of the shape-mode oscillations, several different approaches have been employed. Kang and Lee [28] and Oh et al. [5] add the viscous normal stress term $-2\hat{\mu}\frac{\partial^2\phi}{\partial n^2}$ (where $\hat{\mu}$ denotes dynamic viscosity) and a pressure correction p_v to the normal-stress balance boundary condition. However, in order to determine the pressure correction, the full Navier–Stokes equations have to be considered [28].

Prosperetti [29] developed another approach to deal with the inclusion of viscous effects by also accounting for vorticity in the liquid: an integro-differential equation was derived for the general shape-mode amplitude (the integral part is a convolution integral with respect to the vorticity) together with a partial differential equation for the vorticity. This system reduces to an ordinary differential equation in the shape-mode amplitude only, if the effects of vorticity can be confined to a vanishingly thin layer adjacent to the bubble interface [30]. The viscous terms contained within the later set of ordinary differential equations are the appropriate shape-mode viscous-damping terms for irrotational flow. However, to permit the study of violent bubble collapse with application to the phenomenon of sonoluminescence, we instead employ the approach of Brenner et al. [31]. Though they also work under the constraint of potential flow, they accounted for vorticity by assuming the layer in which it is confined has a finite, but thin, thickness, i.e., the absolute limit of [30] is not applied. Under this assumption modified shape-mode viscous contributions were obtained. The thickness of the assumed boundary layer depends on the diffusion length scale and the order of the shape mode being considered.

For the volume oscillations and the bubble translation we employ the term due to Poritsky [32] and the Levich drag, respectively. These contributions are consistent with a velocity potential flow model. The form of these terms is explicitly given below Eq. 29.

Since we seek conditions under which violent bubble collapse occurs, we assume the van der Waals equation of state for the gas within the bubble [3,31,33]

$$p_g = \left(p_0 + \frac{2\sigma}{R_0}\right)\left(\frac{V_0 - b}{V - b}\right)^{\gamma}, \tag{20}$$

in which the subscript 0 denotes ambient conditions, b is the van der Waals excluded volume ($b = V_0/(8.5)^3$) and γ is the polytropic exponent of the gas. The bubble volume V at time t is determined by conducting an appropriate volume integral, $\int_0^{2\pi}\int_0^{\pi}\int_0^{r_s} r^2\sin\theta\mathrm{d}r\mathrm{d}\theta\mathrm{d}\Psi$, where the bubble surface is defined by (13). Thus

$$p_g = p_{g_0}\left(\frac{R_0^3 - b_1}{R^3 - b_1}\right)^{\gamma} - \epsilon^2 p_{g_0}\gamma\left(\frac{R_0^3 - b_1}{R^3 - b_1}\right)^{\gamma}\sum_{k=2}^{\infty}\frac{3a_k^2 R}{(2k+1)(R^3 - b_1)} + O(\epsilon^3), \tag{21}$$

where $p_{g_0} = p_0 + 2\sigma/R_0$ and $b_1 = 3b/(4\pi)$.

Here, we extend the expression given by Lamb [34, p. 461, Sect. 253] for the surface curvature to include $O(\epsilon^2)$ effects:

$$\nabla\cdot\hat{\mathbf{n}} = \frac{2}{R} + \epsilon\sum_{k=2}^{\infty}(k+2)(k-1)\frac{a_k}{R^2}P_k(\mu) - \epsilon^2\sum_{j=2}^{\infty}\sum_{k=2}^{\infty}(k^2+k-1)\frac{2a_j a_k}{R^3}P_j(\mu)P_k(\mu) + O(\epsilon^3). \tag{22}$$

2.3 System of equations

In order to derive dimensionless differential equations for the bubble dynamics, we introduce the same scalings as Spelt and Matar [3]:

$$[R, a_k, u, t, p, E_0, q] = \left[R_0 R^*, R_0 a_k^*, \sqrt{\frac{\sigma}{\rho R_0}} u^*, \sqrt{\frac{\rho R_0^3}{\sigma}} t^*, \left(\frac{\sigma}{R_0}\right) p^*, E_{00} E_0^*, \overline{\varepsilon}\,\overline{\varepsilon}_0 E_{00} q^* \right], \tag{23}$$

where the star notation indicates a dimensionless quantity and E_{00} is an average electric field strength. We also introduce the dimensionless parameters

$$\begin{aligned} &\mathrm{Oh} = \frac{\hat{\mu}}{\sqrt{\rho\sigma R_0}}, \quad \mathrm{Ma} = \frac{1}{c_\infty}\sqrt{\frac{\sigma}{\rho R_0}}, \quad W = \frac{\overline{\varepsilon}\,\overline{\varepsilon}_0 E_{00}^2}{\sigma/R_0}, \\ &K = \frac{\sqrt{\rho R_0^3/\sigma}}{\overline{\varepsilon}\,\overline{\varepsilon}_0/\kappa}, \quad K_{\mathrm{in}} = \frac{\sqrt{\rho R_0^3/\sigma}}{\overline{\varepsilon}\,\overline{\varepsilon}_0/\kappa_{\mathrm{in}}}, \quad \lambda = \overline{\varepsilon}_{\mathrm{in}}/\overline{\varepsilon}. \end{aligned} \tag{24}$$

These correspond to the Ohnesorge number, the Mach number, the electric Weber number times the relative permittivity of the liquid, dimensionless conductivities and the ratio of the dielectric constants, respectively.

After making use of the identities in the Appendix and equating common terms in the Legendre polynomials, we obtain the following set of dimensionless equations where the star notation has been dropped. The volume oscillation equation is expressed as

$$\begin{aligned} R\ddot{R} + \frac{3}{2}\dot{R}^2 = {} & p_g - p_\infty - \frac{2}{R} + R\mathrm{Ma}\frac{\mathrm{d}}{\mathrm{d}t}\left(p_g - p_\infty\right) - \frac{4\mathrm{Oh}\dot{R}}{R} + f_0(t) \\ & + \epsilon^2\left\{\frac{u_3^2}{4} + \frac{2}{R^3}\sum_{i=2}^{\infty}\sum_{j=2}^{\infty}(j^2+j-1)a_i a_j C_0(i,j)\right\} \\ & + W\left\{\frac{1}{6}\left(2A^2 - 8E_0 A - E_0^2\right) - \epsilon\frac{2a_2}{5R}(A-2E_0)(A-E_0)\right\} \\ & + W\lambda\left\{\frac{1}{6}(E_0+A)^2 + \epsilon(E_0+A)(2E_0+A)\frac{2a_2}{5R}\right\} + O(\epsilon^3). \end{aligned} \tag{25}$$

The translation equation is

$$\begin{aligned} \left(R - \frac{7}{5}\epsilon a_2\right)\epsilon\dot{u}_3 = {} & -\left(3\dot{R} - \frac{12\dot{R}}{5R}\epsilon a_2 - \frac{9}{5}\epsilon\dot{a}_2\right)\epsilon u_3 - \frac{18\mathrm{Oh}}{R}\epsilon u_3 + f_1(t) \\ & + \epsilon^2\frac{4}{R^3}\sum_{i=2}^{\infty}\sum_{j=2}^{\infty}(j^2+j-1)a_i a_j C_1(i,j) \\ & + \epsilon W\frac{12}{5R}\left\{\frac{a_3}{7}\left(A^2 + 11AE_0 - 8E_0^2\right) - (2E_0 - A)\frac{A_2}{R^3}\right\} \\ & + \epsilon W\lambda\frac{4(E_0+A)}{5R}\left\{\frac{A_2}{R^3} + \frac{3a_3}{7}(8E_0+5A)\right\} + O(\epsilon^3). \end{aligned} \tag{26}$$

The P_2 shape-mode amplitude equation is

$$\begin{aligned} & R\epsilon\ddot{a}_2 + 3\dot{R}\epsilon\dot{a}_2 + \left[\frac{12}{R^2} - \ddot{R}\right]\epsilon a_2 + 8\mathrm{Oh}\left[\frac{\epsilon\dot{a}_2}{R}\left(5 - 16\frac{\Gamma}{R}\right) + \frac{\epsilon a_2\dot{R}}{R^2}\left(1 + 4\frac{\Gamma}{R}\right)\right] \\ & = -\frac{9}{4}\epsilon^2 u_3^2 + f_2(t) + g_2(t) + \epsilon^2\frac{6}{R^3}\sum_{i=2}^{\infty}\sum_{j=2}^{\infty}(j^2+j-1)a_i a_j C_2(i,j) \end{aligned}$$

$$+3W\left\{\frac{1}{3}\left(5A^2-2AE_0+2E_0^2\right)+\epsilon(A-2E_0)\frac{12A_3}{7R^5}+\epsilon\frac{4a_4}{21R}\left(5A^2+13AE_0-10E_0^2\right)\right.$$
$$\left.+\epsilon\frac{2a_2}{7R}\left(-13A^2+18AE_0-2E_0^2\right)\right\}+3W\lambda\left\{-\frac{2}{3}(E_0+A)^2+\epsilon(E_0+A)\frac{a_2}{R}\left(\frac{7}{5}A+\frac{4}{7}E_0\right)\right.$$
$$\left.+\epsilon\frac{4a_4}{21R}(E_0+A)(10E_0+7A)+\epsilon\frac{3A_3}{7R^5}(E_0+A)\right\}+O(\epsilon^3). \tag{27}$$

The general shape-mode amplitude equation for $k\geq 3$ is

$$R\epsilon\ddot{a}_k+3\dot{R}\epsilon\dot{a}_k+\left[\frac{(k^2-1)(k+2)}{R^2}-(k-1)\ddot{R}\right]\epsilon a_k+\frac{2\mathrm{Oh}}{R}\left\{\left[(k+2)(2k+1)-2k(k+2)^2\frac{\Gamma}{R}\right]\epsilon\dot{a}_k\right.$$
$$\left.+\frac{\dot{R}}{R}\left[(k-1)(k+2)+2k(k+2)(k-1)\frac{\Gamma}{R}\right]\epsilon a_k\right\}$$
$$=\epsilon^2\frac{2(k+1)}{R^3}\sum_{i=2}^{\infty}\sum_{j=2}^{\infty}(j^2+j-1)a_ia_jC_k(i,j)+f_k(t)+g_k(t)$$
$$+\epsilon W\left\{(A-2E_0)\frac{(k+1)^2(k+2)}{(2k+3)R^{k+3}}A_{k+1}+[A(3k-1)-E_0]\frac{k(k+1)A_{k-1}}{(2k-1)R^{k+1}}\right.$$
$$+\left[A^2(4k-3)+AE_0(9+2k)-E_0^2(6+2k)\right]\frac{(k+1)^2(k+2)}{(2k+3)(2k+5)}\frac{a_{k+2}}{R}$$
$$+\left[A^2(-7k^2-7k+3)+AE_0(10k^2+10k-6)-E_0^2k(k+1)\right]\frac{2(k+1)}{(2k-1)(2k+3)}\frac{a_k}{R}$$
$$\left.+(1-\delta_{3k})\left[-(4k+7)A^2+(7-2k)AE_0+2(k-2)E_0^2\right]\frac{k(k^2-1)}{(2k-3)(2k-1)}\frac{a_{k-2}}{R}\right\}$$
$$+\epsilon W\lambda(E_0+A)\left\{\frac{(k+1)^2A_{k+1}}{(2k+3)R^{k+3}}-\frac{2k(k^2-1)A_{k-1}}{(2k-1)R^{k+1}}\right.$$
$$+\frac{a_{k+2}}{R}\frac{(k+1)^2(k+2)}{(2k+3)(2k+5)}[A(2k+3)+2E_0(k+3)]+\frac{a_k}{R}\left[\frac{2E_0k(k+1)^2}{(2k-1)(2k+3)}+\frac{A(k^2-1)(3k+1)}{2k+1}\right]$$
$$\left.+(1-\delta_{3k})\frac{a_{k-2}}{R}\frac{k(k^2-1)}{(2k-1)(2k-3)}[2A(2k-1)-2E_0(k-2)]\right\}+O(\epsilon^3); \tag{28}$$

details of the determination of the electrostatic contributions to the normal-stress balance can be found in the Appendix.

In the above equations, the terms $f_k(t)$ $(k\geq 0)$ and $g_k(t)$ $(k\geq 2)$ are given by Eqs. 2.26 and 2.27 in Doinikov [25], respectively (allowing for the notation used within his paper), although here the $O(\epsilon^2)$ correction to the pressure inside the gas is that for the van der Waals model and is contained within the term p_g in (25). Thus $f_k(t)$ is

$$f_k(t)=\epsilon^2\sum_{l=2}^{\infty}\sum_{m=2}^{\infty}\left\{a_la_m\left[\frac{\ddot{R}}{R}\alpha_1(k,l,m)+\frac{\dot{R}^2}{R^2}\alpha_2(k,l,m)\right]+\alpha_3(k,l,m)\ddot{a}_la_m\right.$$
$$\left.+\alpha_4(k,l,m)\frac{\dot{R}}{R}(\dot{a}_la_m+\dot{a}_ma_l)+\alpha_5(k,l,m)\dot{a}_l\dot{a}_m\right\}. \tag{29}$$

The coefficients $\alpha_1(k,l,m)-\alpha_5(k,l,m)$ are given by (2.28)–(2.32) in Doinikov [25]. We do not repeat these terms here or the expression for $g_k(t)$ again for clarity of presentation. Within (27) and (28), the contributions multiplied by the Ohnesorge number, Oh, are the viscous shape-mode damping terms due to Brenner et al. [31]. Within these terms Γ characterises the momentum boundary-layer thickness for each shape mode and is defined by $\Gamma=R/2k$, $k\geq 2$ [31]. The volume oscillation damping term is $4\mathrm{Oh}\dot{R}/R$, while the Levich drag is $18\mathrm{Oh}\epsilon u_3/R$. The coefficients

$C_k(i,j)$ denote the square of the Clebsch–Gordan coefficients. The pressure inside the bubble now has the form

$$p_g = \Pi_0 \left(\frac{1-b_1^*}{R^3-b_1^*}\right)^\gamma - \epsilon^2 \Pi_0 \gamma \left(\frac{1-b_1^*}{R^3-b_1^*}\right)^\gamma \sum_{k=2}^{\infty} \frac{3a_k^2 R}{(2k+1)(R^3-b_1^*)} + O(\epsilon^3), \tag{30}$$

where $\Pi_0 = p_0 + 2$ and $b_1^* = 1/(8.5)^3$.

To the order of analysis considered within this work, the term $\nabla_S \cdot (q\mathbf{u}_S)$ has the form

$$\begin{aligned}\nabla_S \cdot (q\mathbf{u}_S) &= \left[\nabla \cdot \left(q(\mathbf{u} - \hat{\mathbf{n}}(\hat{\mathbf{n}} \cdot \mathbf{u}))\right)\right]_S - \left[\hat{\mathbf{n}} \cdot \{(\hat{\mathbf{n}} \cdot \nabla)(q(\mathbf{u} - \hat{\mathbf{n}}(\hat{\mathbf{n}} \cdot \mathbf{u})))\}\right]_S \\ &= \epsilon \frac{\hat{q}}{R} \left\{ 3u_3 P_2 - \sum_{k=1}^{\infty} \frac{k(k+1)}{2k+3} \left[k a_{k+1} \frac{\dot{R}}{R} - \dot{a}_{k+1} \right] P_k \right. \\ &\quad \left. - \sum_{k=3}^{\infty} \frac{(k-1)(k+1)}{2k-1} \left[(k-2) a_{k-1} \frac{\dot{R}}{R} - \dot{a}_{k-1} \right] P_k \right\} + O(\epsilon^2),\end{aligned} \tag{31}$$

while the contribution from the second term on the right-hand side of (6) is

$$\mathbf{u}_n \cdot \nabla q = -\frac{\epsilon \hat{q} \dot{R}}{R^2} \left[\sum_{k=1}^{\infty} \frac{(k+1)(k+2)}{2k+3} a_{k+1} P_k - \sum_{k=3}^{\infty} \frac{k(k-1)}{2k-1} a_{k-1} P_k \right] + O(\epsilon^2). \tag{32}$$

Adding the contributions from (31) and (32) to the boundary condition (4) gives rise to the following dimensionless interfacial charge-density components

$$\begin{aligned}\dot{\hat{q}} &= -K(E_0 - 2A) + K_{\text{in}}(E_0 + A) - \frac{2\dot{R}}{R}\hat{q} \\ &\quad + \epsilon \frac{6a_2}{5R} \left[K(E_0 - A) - K_{\text{in}}(E_0 + 2A) - \frac{4\dot{R}\hat{q}}{3R} \right] - \epsilon \frac{4\hat{q}}{5R} \dot{a}_2 + O(\epsilon^2),\end{aligned} \tag{33}$$

$$\begin{aligned}\epsilon \dot{\hat{q}}_2 &= \epsilon \left\{ K \left[\frac{6a_3}{7R}(2E_0 - A) + \frac{3A_2}{R^4} \right] + K_{\text{in}} \left[-\frac{6a_3}{7R}(2E_0 + 5A) + \frac{2A_2}{R^4} \right] - \frac{2\dot{R}}{R}\hat{q}_2 \right. \\ &\quad \left. - \frac{6\dot{R}}{7R^2}\hat{q}a_3 - \frac{12\hat{q}}{7R}\dot{a}_3 - \frac{3\hat{q}u_3}{R} \right\} + O(\epsilon^2),\end{aligned} \tag{34}$$

and for $k \geq 3$

$$\begin{aligned}\epsilon \dot{\hat{q}}_k &= \epsilon \left\{ K \left[-\frac{6A}{R}\xi_k + \frac{(k+1)A_k}{R^{k+2}} + (E_0 + A)\frac{\zeta_k}{R} \right] \right. \\ &\quad + K_{\text{in}} \left[-\frac{3kA}{R}\xi_k + \frac{kA_k}{R^{k+2}} - (E_0 + A)\frac{\zeta_k}{R} \right] \\ &\quad - \frac{2\dot{R}}{R}\hat{q}_k - \frac{\dot{R}\hat{q}}{R^2} \frac{2(k+1)(k-1)}{2k+3} a_{k+1} - \frac{\hat{q}(k+1)(k+2)}{R(2k+3)} \dot{a}_{k+1} \\ &\quad \left. - \frac{2\dot{R}\hat{q}}{R^2} \frac{(k^2-k-1)}{2k-1} a_{k-1} - \frac{\hat{q}(k^2+2k-1)}{(2k-1)R} \dot{a}_{k-1} \right\} + O(\epsilon^2).\end{aligned} \tag{35}$$

Here ξ_k and ζ_k are expressed by

$$\xi_k = \frac{k+1}{2k+3} a_{k+1} + (1 - \delta_{2k}) \frac{k}{2k-1} a_{k-1}, \tag{36}$$

$$\zeta_k = \frac{(k+1)(k+2)}{2k+3} a_{k+1} - (1 - \delta_{2k}) \frac{k(k-1)}{2k-1} a_{k-1}, \tag{37}$$

in which δ_{ij} is the Kronecker delta function.

In order to obtain expressions for the dimensionless coefficients A and A_k, we substitute the expansions given by (14) and (15) in the dimensionless versions of the interfacial conditions (2) and (3), which, after making use of

identities given in the Appendix and equating coefficients in the resultant Legendre polynomials, yields

$$A = \frac{1}{\lambda+2}\left[-\hat{q} + E_0(1-\lambda) - \epsilon\frac{6a_2}{5R}\left\{\left(\frac{1+2\lambda}{\lambda+2}\right)\hat{q} + E_0\frac{(\lambda-1)^2}{\lambda+2}\right\}\right] + O(\epsilon^2),$$

$$\epsilon A_k = \epsilon\frac{R^{k+2}}{(k+1)+\lambda k}\left[-\hat{q}_k - \frac{\hat{q}}{R(\lambda+2)}\{3\xi_k(2+k\lambda) - \zeta_k(1-\lambda)\} + \frac{3E_0(1-\lambda)}{R(\lambda+2)}\{\xi_k(2+k\lambda) - \zeta_k\}\right] + O(\epsilon^2). \tag{38}$$

In deriving the above system of equations, we have assumed that $W = O(\epsilon)$. Consequently, we shall choose sufficiently small values for W such that a_2 remains of order ϵ, which is taken to be approximately equal to 0.1, in the present study. Our equations extend the work of Doinikov [25] in order to include low-Mach-number compressibility effects, surface-tension effects to quadratic order in the small-interaction terms and shape-mode viscous damping, but have omitted the spatially varying acoustic-field contributions. We have also used a van der Waals rather than a perfect gas equation of state to model the behaviour of the gas within the bubble. Previous work on the dynamics of a bubble in a uniform electric field has also been constrained to the case of small ellipsoidal deformation only. Thus, all the electric-field contributions in the translation equation (26) and the general shape-mode amplitude equation (28) for $k \geq 3$ are new. Within the volume oscillation equation (25) and the P_2 shape-mode amplitude equation (27), the electric-field terms are consistent with those presented by Spelt and Matar [3], although (27) has been extended to include contributions from the P_4 shape mode. We also observe that in the absence of any interfacial charge density as the bubble dynamics evolves, at leading order, the electric-field contributions within the volume oscillation and P_2 shape-mode equation are $\frac{3}{2}WE_0^2\frac{\lambda-1}{\lambda+2}$ and $9WE_0^2\frac{(\lambda-1)^2}{(\lambda+2)^2}$. These respective terms are the electric-field contributions used by Oh et al. [5] in their study of a bubble in a dielectric liquid under a uniform electric field.

2.4 Discussion of the model equations

Here, we make tentative predictions regarding the behaviour of the bubble in various limiting cases via inspection of the above system of nonlinear ordinary differential equations (ODEs) governing the bubble dynamics. Note that we concentrate on the new interactions offered by the electric-field effects. Consider the case of an initially stationary, uncharged, non-oscillating, spherical bubble. Upon switching on an electric field of magnitude E_0, the bubble is instantaneously set into volume oscillations, undergoes surface deformation with respect to the P_2 shape mode, and acquires an interfacial charge density consisting of the component $\hat{q}$ provided $\lambda > 0$. The equations indicate that, even to linear order in ϵ, these effects are strongly coupled. At the same time, higher-order shape modes become excited and other charge-density components can become non-zero. In particular, if the P_k shape mode is deformed then, in the presence of an electric field, this mode will excite the P_{k+2} and the P_{k-2} shape modes. Thus for an initially stationary, spherical bubble we have that the P_2 shape mode will excite the P_4 shape mode which, in turn, excites the P_6 (and P_2) shape mode which then excites the P_8 (and P_4) mode and so on. Clearly energy is transferred to higher even shape modes via a cascade effect and no odd shape modes are excited through this set of interactions.

Numerical work for both bubbles and drops undergoing free oscillations as a result of an initial distortion in shape [35,36] has predicted that, if this distortion is in terms of an even shape mode, other even shape modes become excited, but odd shape modes do not; this is in agreement with the above observations. In the case of a bubble, the equations of Doinikov [25] clearly show that, to second order in the small-interaction terms, even shape modes only excite other even shape modes and the equations of Shaw [37] show that this also holds at third order. Thus, one can therefore conclude that, to the order of interactions considered within this paper (and the physical mechanisms accounted for), there appears to be no mechanism for exciting odd shape modes in the case of an initially stationary, uncharged spherical bubble. If, instead, the bubble is initially charged, it is noted that the P_k shape mode will become excited if either the $\hat{q}$, $\hat{q}_{k-1}$ or $\hat{q}_{k+1}$ charge-density components are non-zero.

In the work of Doinikov [25], it was noted that odd shapes modes will be excited by a moving bubble or the action of a spatially varying acoustic pressure field. The same is expected for a spatially varying electric field, although

this will not be demonstrated here. A further consequence of the above observations is that the application of a spatially uniform electric field to an initially stationary, uncharged, spherical bubble will not result in translation. Equation (26) indicates that, if we wish to move a bubble using such an electric field, the bubble must either be deformed in terms of the P_3 Legendre polynomial or have a non-zero interfacial charge-density component $\hat{q}_2$. Further inspection of the equations reveals that this can be generalised to any odd shape-mode deformation or even interfacial charge-density term. As a consequence of the modal interactions identified above, then an initial distortion in any general odd shape mode, in turn, causes the excitement of the P_3 shape mode via the cascade effect and bubble translation ensues. The same argument applies to an initially non-zero, general even interfacial charge-density term. This set of identified interactions provides one means by which energy can be transferred to result in bubble translation. It is noted that modal excitement can also occur via higher-order interactions in ϵ, but by their nature these interactions are expected to be less significant, except when the deformation becomes large. In the absence of an electric field, it is well established that quadratic interactions between odd and even shape modes can cause bubble movement [25,38,39]. It has also been shown [25,37] that an initially non-zero odd shape mode can excite both odd and even shape modes via terms which are not coupled to an electric field.

In the case of the charge density, the ODEs indicate that the $\hat{q}_k$ component will become non-zero if either the P_{k-1} or P_{k+1} shape mode has a non-zero amplitude. Thus, for an initially stationary, uncharged spherical bubble as the even shape modes become excited sequentially in k, this will correspondingly cause the odd number components of interfacial charge density to become non-zero, i.e., upon excitement, the P_2 shape mode will cause the $\hat{q}_3$ charge-density term to become non-zero, the P_4 shape mode will cause the $\hat{q}_5$ charge density term to become non-zero and so on. The system of equations (25)–(28), (33)–(35), (38) indicates that, once particular shape-mode amplitudes and charge-density components become non-zero, coupling between these terms will, of course, cause modification. It is also clear that the volume oscillations of the bubble together with the non-electric field effects will cause further modification.

3 Results

In this section, we present a selection of our results. The effect of electric forcing on the steady and time-dependent solutions of Eqs. 25–28, 33–35 is examined, where attention is restricted to $E_0 = 1$. We begin, however, with a concise description of the numerical procedure used to carry out the computations. Note that the hat notation used with respect to the charge-density components is suppressed for the remainder of this work. Also note that for purposes of presentation the small parameter ϵ is absorbed into the appropriate perturbation terms, i.e., assume henceforth $u_3 \equiv \epsilon u_3$; $a_k \equiv \epsilon a_k$, for $k \geq 2$; $q_k \equiv \epsilon q_k$ for $k \geq 2$, etc.

3.1 Numerical procedure

In order to determine how the bubble dynamics and charge-density components evolve in time for a given set of parameters and initial conditions, the system of ODEs (25)–(28), (33)–(35) must be solved using numerical techniques. First, attention is restricted to the first N Legendre terms only. Making use of the symbolic manipulation package MAPLE, the truncated ODE system is then solved in the manner of Shaw [37] to obtain expressions for $\ddot{R}, \dot{u}_3, \ddot{a}_k, \dot{q}$ and $\dot{q}_k$ to $O(\epsilon^2)$, where $2 \leq k \leq N$. At this stage, the coefficients A and A_k are eliminated by employing relations (38). The resultant equations are numerically integrated using a fourth-order accurate Runge–Kutta method. Note that prior to integration, the pertinent terms within these equations were compared with (27)–(31) of the inviscid, incompressible free-oscillation work of Shaw [37] and were found to be consistent. We have also ensured that the results of Spelt and Matar [3] are recovered in the appropriate limit; an explicit comparison is given at the beginning of the transient-results section. Additional checks were performed by ensuring that the predictions of the numerical procedure are in excellent agreement with steady solutions of the nonlinear system of

ODEs, obtained using MAPLE. A full parametric study is beyond the scope of this paper; we focus instead on three problems involving higher shape-modes contributions.

3.2 Steady solutions

The first results considered are a set of steady-state solutions of the governing ODEs. The highly nonlinear algebraic equations resulting from the steady versions of (25)–(28), (33)–(35) admit a large number of solutions (which increases with γ due to the increase in nonlinearity of the equations), and only solutions in the real domain are considered that satisfy $R > b_1^*$, $(|a_k|, |q_k|) < 0.35$, for $k \geq 2$. Spelt and Matar [3] identified two main solution branches which the present analysis confirms. Increasing the truncation parameter N, i.e., the number of Legendre terms retained, causes small modifications to these branches, although as W increases so does the size of these modifications. A third branch was determined in the present analysis which was found to be much more sensitive to the value of N.

In Fig. 1a and b, the effect of varying W on the lower solution branch of Spelt and Matar [3] together with the newly identified third branch (upper set of curves in both pictures) for R and a_2 are plotted for $\Pi_0 = 1$ and $\Pi_0 = 2$. These results were generated using $\lambda = 0.1$, $\gamma = 1$ and $(K, K_{\text{in}}) = (1, 0)$. It is seen that, as Π_0 is increased, the third solution branch becomes admissible for an increasingly larger range of W values. At $\Pi_0 = 2$, a corresponding solution is found at $W = 0$. This branch was found to converge to almost the same radius as the lower branch, but all shape modes are rather large and the convergence of this branch with respect to N is slow. As also shown in Fig. 1c, which depicts the shape-mode amplitudes for the three identified solution branches at $W = 0.3$, $\Pi_0 = 0.75$, $(K, K_{\text{in}}) = (4.67 \times 10^{-3}, 0)$, the shape-mode amplitudes associated with the upper and lower branches appear to

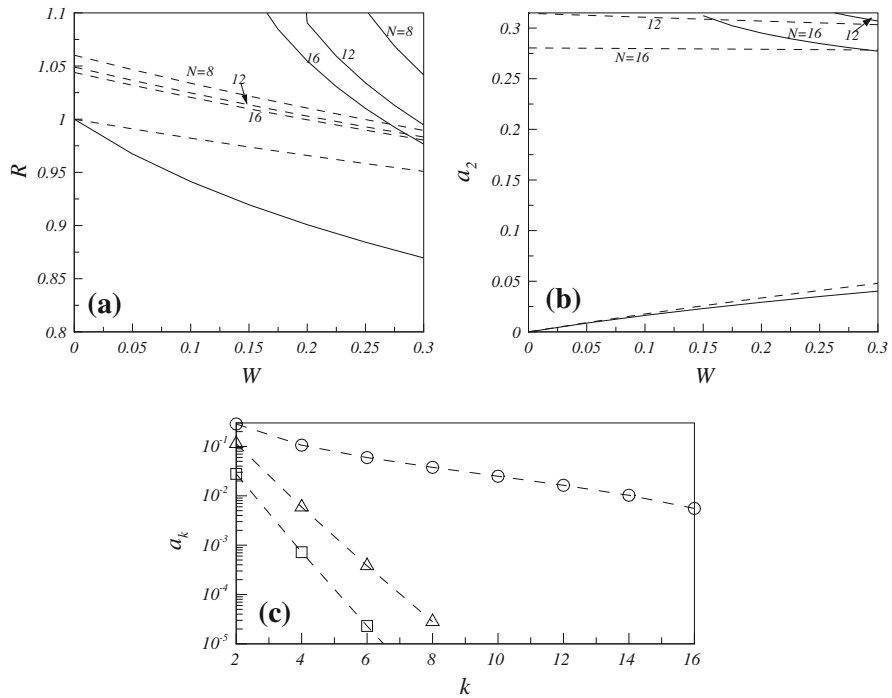

Fig. 1 Steady-state bubble radius, (**a**), and first shape mode, (**b**), as a function of W for different values of Π_0; $\Pi_0 = 1$ (*solid lines*) and 2 (*dashed line*) while $\lambda = 0.1$, $\gamma = 1$, $(K, K_{\text{in}}) = (1, 0)$, Oh = 0.037 and Ma = 1.81×10^{-3}; only the 'lower' and 'third' branches are shown (see text). **c** Steady-state bubble shape-mode amplitudes as a function of mode number for the three solution branches with $W = 0.3$, $\Pi_0 = 0.75$, $\lambda = 0.1$, $\gamma = 1$ and $(K, K_{\text{in}}) = (4.67 \times 10^{-3}, 0)$; the *squares*, *triangles* and *circles* represent the 'lower', 'upper' and 'third' branches, respectively. All odd modes are zero, and the dashed lines in panel (**c**) are included for illustrative purposes

decay approximately exponentially to zero with increasing k; those associated with the third branch, however, decay at a distinctly slower rate. We point out here that the aspect ratio of the bubble is close to $\sqrt{2}$ in this case; Kushch et al. [40] showed that, beyond this value, spherical harmonics are not convergent, and ellipsoidal harmonics should be used instead. Note that for all the cases considered in this section, the respective amplitudes of all the odd shape modes, together with the even charge-density components and any bubble translation were found to be zero. This is consistent with the observations made in Sect. 2.4.

3.3 Transient solutions

We begin the discussion of our time-dependent results by comparing our predictions with those of Spelt and Matar [3] who did not account for nonlinear interactions between the shape modes (or bubble translation). As shown in Fig. 2, for the parameter set as indicated, the agreement is good with small discrepancies only really becoming apparent in a_2 and q_3 at long times. These discrepancies are expected to grow with increasing W.

In Fig. 3, we display the evolution of the volume oscillations, the first four even shape-mode amplitudes and the first two odd charge-density components for different values of λ. Consistent with our observations in Sect. 2.4 all odd shape modes together with even charge-density charge components remain zero-valued, as does the bubble velocity (not shown). The amplitude of the oscillations in R and the even shape modes increase with decreasing λ, becoming largest in the limit of $\lambda \to 0$. This is because the contrast in dielectric constants increases with decreasing λ which promotes the electric contribution to the dynamics. This is in agreement with the results of Spelt and Matar [3], who showed that increasing λ results in an increase in the final steady value of R. It is also evident that an increase in λ results in a concomitant rise in the growth rate of q and q_3, and q reaches a steady value, which is in agreement with the asymptotic relation derived by Spelt and Matar [3], $q \sim -3\lambda/2$, and is negative since $K_{\text{in}}/K \to 0$; this occurs on a much longer time scale than that needed for R and the shape modes to reach steady state. In order to rationalise this feature, we considered (33) in the limit $K_{\text{in}} \to 0$ and exploited the fact

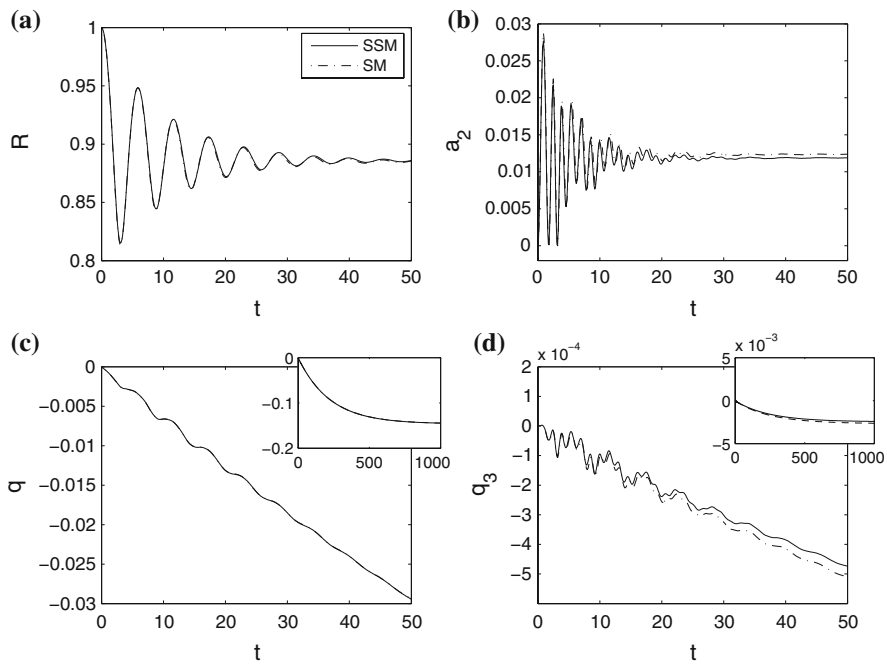

Fig. 2 Comparison of the predictions of the present theory with those of Spelt and Matar [3], labeled 'SSM' and 'SM', respectively, for R, a_2, q and q_3, starting from $R(0) = 1$; $\Pi_0 = 0.75$, $\lambda = 0.1$, $\gamma = 1$, $(K, K_{\text{in}}) = (4.67 \times 10^{-3}, 0)$ and $W = 0.11$. The insets show the long-time behaviour of q and q_3

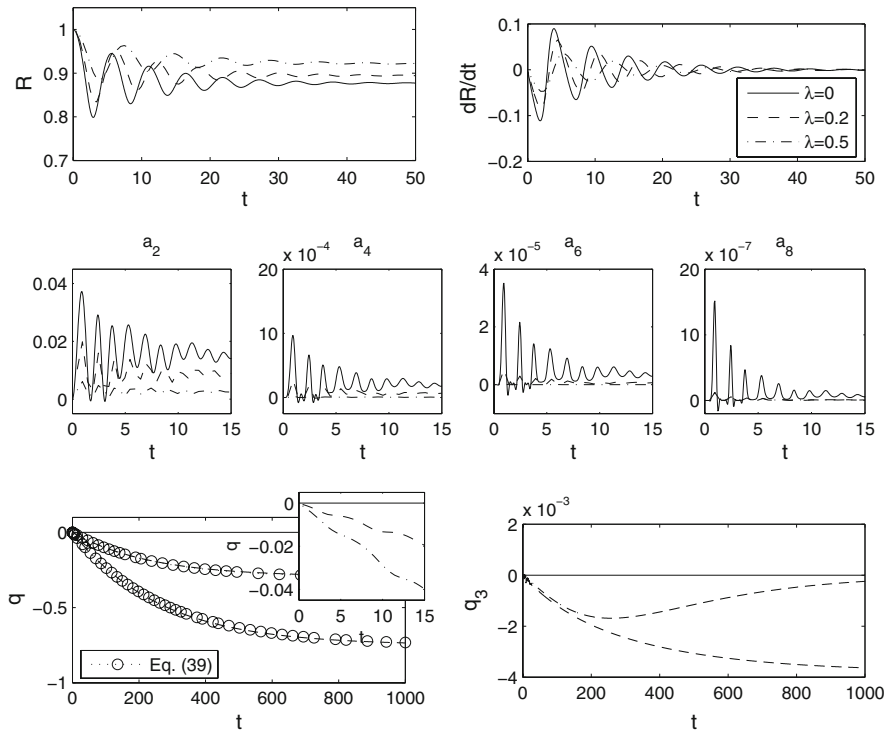

Fig. 3 The effect of varying λ on the dynamics with $W = 0.11$, $\Pi_0 = 0.75$, $(K, K_{\text{in}}) = (4.67 \times 10^{-3}, 0)$, Oh = 0.037 and Ma = 1.81×10^{-3}. Also shown are the predictions of (39) for q

that $\dot{R} \to 0$ on a relatively fast time scale. We also note that we have set $E_0 = 1$. Hence, $\dot{q} \approx -K(1 - 2A)$, with $A \approx (-q + [1 - \lambda])/(\lambda + 2)$, to leading order in ϵ, and thus

$$q \approx -\frac{3}{2}\lambda \left(1 - \mathrm{e}^{-2Kt/(2+\lambda)}\right). \tag{39}$$

The agreement between the full numerical solution and the predictions of this simple analytical expression for q is excellent, as shown in Fig. 3. Also, inspection of (39) reveals that an increase in K and a decrease in λ lead to a faster decay towards the steady solution.

The effect of viscous damping is clearly seen in Fig. 3 as the volume oscillations, bubble translation and shape-mode oscillations undergo significant decay. Indeed, as expected, as the order of the shape modes increases the timescale over which the observed oscillatory motion is damped increases, with the resultant steady states being achieved sooner.

In Fig. 4, we show contour plots of the magnitude of the electric field (with field lines superimposed), pressure and the magnitude of the velocity field (again with field lines superimposed). These were generated with the same parameter values as in Fig. 3 and for $\lambda = 0$. The chosen time corresponds to the early stages of re-expansion after the first minimum in the bubble radius, $R(t)$. The observed form of the electric field is explained by noting that for $\lambda = 0$, no charge is induced on the bubble surface. Therefore at leading order $A = 1/2$ and $B = 3/2$ which are the first coefficients in the respective electric field Fourier–Legendre expansions (14), (15). Note, for the field outside the bubble, by the form of the expansion, the P_1 contribution is forced towards zero along the symmetry line, on the bubble surface. As the bubble is near the first minimum volume, then the contents are clearly shown to be under compression relative to the surrounding water. Also, during this stage of the re-expansion, the P_2 shape mode has a higher velocity than the spherical bubble radius.

A typical charge-density distribution on the bubble surface is shown in Fig. 5, for the parameter set of Fig. 3 and for $\lambda = 0.01$. Note, the orientation of this figure is such that the electric field is from the right to left in this case.

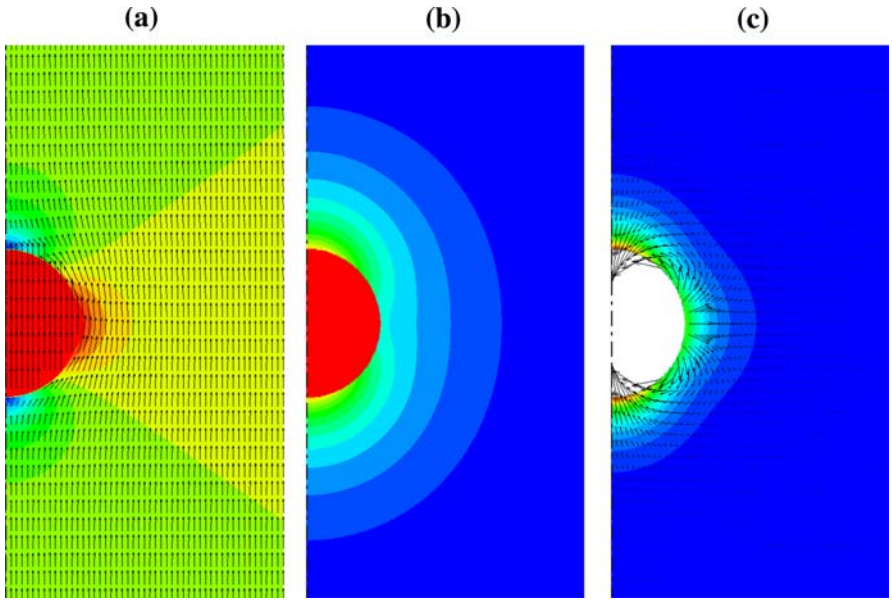

Fig. 4 Contour plots of the magnitude of the electric field, pressure and magnitude of the velocity field shown in (**a**)–(**c**), respectively, for $\lambda = 0$ and $t = 2.95$; the rest of the parameters are the same as those used to generate Fig. 3. Superimposed on (**a**) and (**c**) are the corresponding field lines. The respective contour ranges are 0–1.5 in (**a**); −1.2 to 1 in (**b**); in (**c**) 0.002–0.036

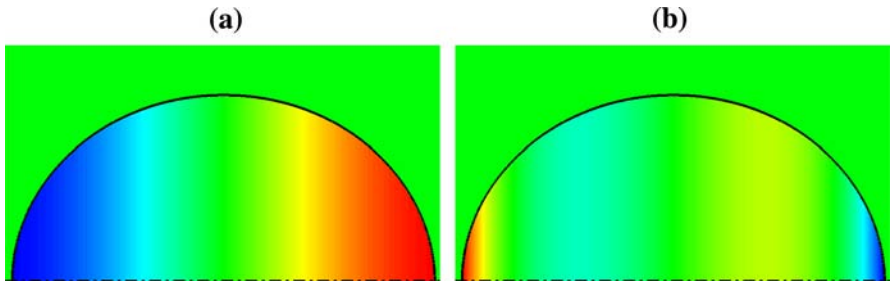

Fig. 5 Bubble shape and charge-density plots for $\lambda = 0.01$ and $t = 0.849$; the rest of the parameters are the same as those used to generate Fig. 3. The applied electric field is from right to left. **a** The sum of all charge-density components; **b** the same as (**a**), but not including $P_1 q$

Although the P_1 charge-density distribution dominates, deviations are significant at the left and right most parts of the bubble.

In Fig. 6, we show the early-time dynamics of R, the first six shape modes, the displacement, x_3, the translational velocity, u_3, q and the first six higher components of the interfacial charge density; this plot was generated with the same parameters as those used in Fig. 3 except $\Pi_0 = 0.22$, Oh = 0.01 and the simulations began from an amplitude of 10^{-4} for all the variables. Here, we have chosen a lower value of Π_0 deliberately since, based on parametric studies (not shown) and the steady-state solutions shown in Fig. 1, we would expect a more rapid transition towards a lower, steady bubble radius, and, therefore, a greater response with decreasing Π_0. Inspection of panels (a) and (d) of Fig. 6 reveals that the rapid collapse of the bubble radius from $R(0) \approx 1$ to near its steady value is accompanied by bubble translation, which appears to be intimately coupled to the build-up of interfacial charge; this, in turn, is strongly coupled to the bubble dynamics and its oscillations are synchronous with the after-bounces of the bubble. As shown in panels (b), (c), (e) and (f) of Fig. 6, the magnitude of bubble deformation and the amplitude of the higher components of the interfacial charge density also undergo rapid increase during the final stages of each collapse which occurs on short time scales. We also note that the higher-order shape modes decay faster than the lower-order

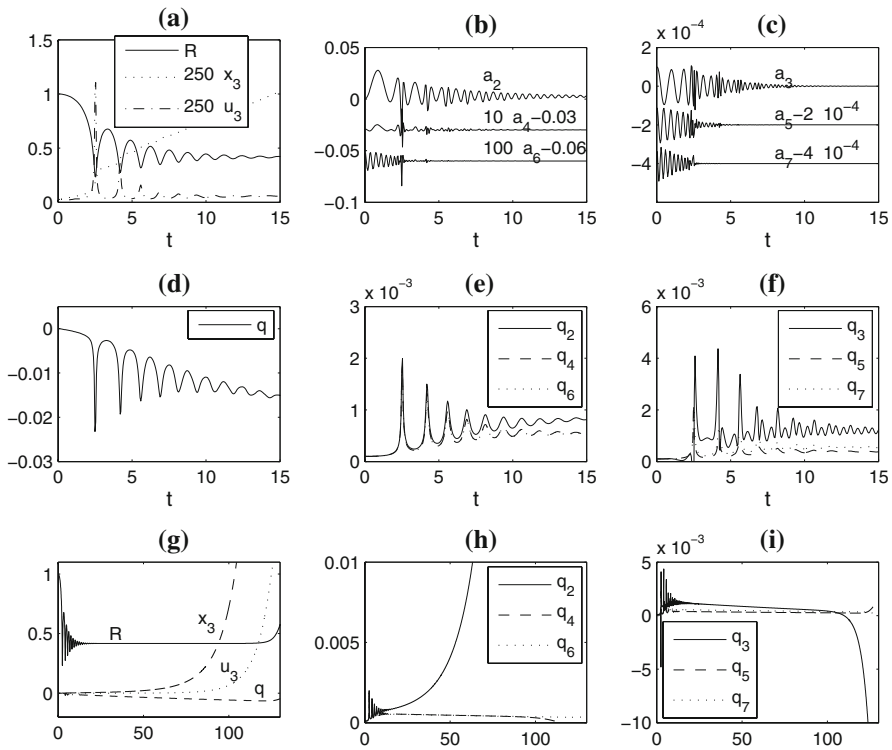

Fig. 6 Evolution of R, the first six shape modes and translational velocity, u_3, shown in (**a**)–(**c**), and q as well as the first six higher components of the interfacial charge density, (**d**)–(**f**) starting from an amplitude of 10^{-4} for all variables; $W = 0.11$, Oh = 0.01, Ma = 0.0181, $\lambda = 0.1$ and $\Pi_0 = 0.22$. In (**g**)–(**i**) long-time dynamics of R, q, x_3 u_3 and the first six higher components of the interfacial charge density

ones and their dynamics exhibit two separate stages: the first occurs at early times and the second coincides with the latter stages of the first rapid collapse. The interfacial charge density also exhibits interesting dynamics: the magnitude of q and the first six higher components exhibit local maxima which coincide with each collapse, and the magnitude of the odd charge-density components exceeds that of the even ones; although q remains negative throughout, the other modes are all positive.

Also shown are the long time dynamics of R, u_3 and the charge-density components. Here, it is seen that q_2 undergoes a rapid increase, which is followed by a rise in x_3 and u_3, and an increase in the magnitude of q_3. The charge density q does not exhibit a discernible change from the behaviour dictated by (39), while R remains steady until relatively late stages of the flow when it undergoes a sharp increase. This increase in the magnitude of the higher-order modes heralds the breakdown of the asymptotic theory. Nevertheless, this is indicative of an instability that leads to the continual increase in the value of R.

It proves instructive to derive a simple system of equations, which can be examined more easily than the full set derived in the previous section, in order to determine the mechanism underlying the behaviour show in Fig. 6. Guided by the results shown in this figure, we assume that near the onset of the growth of q_2, $q \approx -\frac{3}{2}\lambda\left(1 - \mathrm{e}^{-2Kt/(2+\lambda)}\right)$, $R = R_s$, which corresponds to the steady value reached by the bubble radius following the early time dynamics shown in Fig. 6a. We also assume that a_2 and a_3 are negligibly small (or at least enter the analysis at the next order) and set $K_{\mathrm{in}} = 0$. As a result, $A_2 \approx -R_s^4 q_2/(3 + 2\lambda)$ and the equation governing the dynamics of q_2 reduces to

$$\dot{q}_2 = -\frac{3K}{(3+2\lambda)}q_2 - \frac{3q}{R_s}u_3. \tag{40}$$

The equation for u_3 also reduces to

$$\dot{u}_3 = -\frac{18\mathrm{Oh}}{R_s^2}u_3 - \frac{4Wq_2}{5(3+2\lambda)R_s}\left[-\frac{3(2\lambda+3)}{\lambda+2} - \frac{\lambda+3}{\lambda+2}q\right], \tag{41}$$

where the reduction $A \approx (1-\lambda-q)/(\lambda+2)$ has been applied. Inspection of (40) and (41) reveals that decay in q_2 and u_3 results from the first terms on the right-hand side of these equations; these are related to the conductivity of the outer fluid and its viscosity, respectively. The second term on the right-hand side of (40) can result in growth as Fig. 6 indicates q is negative while u_3 is positive. In (41) the contribution from q couples with q_2 to cause further decay, while the remaining term on the right-hand side involving the q_2 component solely causes growth. Therefore, the key interaction is the term $-3qu_3/R_s$ in (40). Provided u_3 is not damped to zero, growth in $-q$ will eventually cause q_2 to blowup which will then trigger the blowup of the bubble velocity. At this point the theory becomes invalid, though the indications are that strong growth in the bubble volume then occurs, followed later by shape distortion. However, in order to confirm this a new model permitting $O(1)$ amplitudes in u_3 and q_2 would be required.

If we assume $q \to -\frac{3\lambda}{2}$, i.e., the steady-state limit, then the eigenvalues for the coupled system (40), (41) are

$$\frac{1}{2}\left\{(\beta_1+\beta_4) \pm \sqrt{(\beta_1+\beta_4)^2 - 4(\beta_1\beta_4 - \beta_2\beta_3)}\right\}, \tag{42}$$

where

$$\beta_1 = -\frac{3K}{3+2\lambda}, \quad \beta_2 = \frac{9\lambda E_0}{2R}, \quad \beta_3 = W\frac{6E_0(3-\lambda)}{5(3+2\lambda)R}, \quad \beta_4 = -\frac{18\mathrm{Oh}}{R^2}. \tag{43}$$

Hence a necessary condition for instability is

$$\frac{W}{\mathrm{Oh}\,\mathrm{K}} > \frac{10}{\lambda(3-\lambda)}. \tag{44}$$

This condition is indeed met in the case studied in Fig. 6; we have also completed further tests on the full system of equations, all of which confirm this condition, including cases which are stable under (44). We have verified that for the case studied in Fig. 6 the growth rate of u_3 and q_2 is below that predicted by (42), as expected, given that q has not reached its equilibrium value for the time domain shown (and these would become too large for the analysis to be valid once it does). We have verified that the term that causes the instability (the second term on the right-hand side of (40)), corresponds to the first term on the right-hand side of (5), i.e., the charge advection on the bubble surface.

In summary, then, if condition (44) is met, and u_3 is slightly perturbed (or a given mode which subsequently causes u_3 to become excited, as discussed in Sect. 2.4), then as q decreases gradually towards its supposed equilibrium value, one of the eigenvalues of (42) becomes positive due to charge advection on the bubble surface. In turn this triggers the dramatic growth in translation of the bubble and possible subsequent break-up or transition to a new quasi-steady state.

4 Conclusions

A theoretical model has been derived for the nonlinear dynamics of a gas bubble in a low-Mach-number, weakly viscous dielectric liquid which is being forced by a spatially uniform electric field. Representing any shape deformation of the bubble by a sum of spherical harmonics together with any induced charge density, domain perturbation analysis is applied with respect to the bubble-surface boundary conditions, wherein any translation or shape deformation of the bubble is assumed small, but no restriction is imposed on the volume oscillations. The equations presented include interactions in the perturbation terms to quadratic order that have allowed us to extend the range of W values (ratio of electric to surface-tension stresses) for which steady-state shapes could be investigated beyond that studied by Spelt and Matar [3]. Our analysis of the equations suggests that, unless a bubble is initially deformed in terms of at least one odd shape mode or acquires an even component of interfacial charge density, then only even

shape modes and odd charge-density components will be excited. This is confirmed by our numerical simulations. The two steady-state branches identified by Spelt and Matar [3] are confirmed; increasing the number of terms included in the spherical-harmonic expansions causes only small modifications. A third steady-state branch is also identified which is found to be much more sensitive to the later expansions' truncation. In the case of time-dependent solutions, our numerical results also show that, when all shape modes and interfacial charge-density components are excited, bubble translation occurs; this is found to be directly related to the build-up of charge at the interface. At later stages in the dynamics, a coupling of this charge build-up and bubble translation gives rise to an instability that leads to bubble acceleration and a sudden increase in the radius, caused by charge advection on the bubble surface. We speculate that this may ultimately lead to bubble break-up, but caution that a more elaborate account of viscous effects and large shape deformation may be needed in this context. Contour plots of the magnitude of the electric field, pressure and the magnitude of the velocity within the bubble and the surrounding liquid are shown for one example; bubble shape and charge-density plots are also given.

For future work, full numerical simulations are recommended, together with a more developed theory for the potential bubble break-up.

Acknowledgment The authors would like to acknowledge financial support from EPSRC under grant EP/D50371X/1.

Appendix

Identities

The following set of Legendre polynomial relations have been used as a part of the derivations presented in this paper.

$$P_1^2 = \frac{1}{3}P_0 + \frac{2}{3}P_2, \tag{45}$$

$$\left(\frac{\mathrm{d}P_1}{\mathrm{d}\theta}\right)^2 = (1-\mu^2)\left(\frac{\mathrm{d}P_1}{\mathrm{d}\mu}\right)^2 = \frac{2}{3}P_0 - \frac{2}{3}P_2, \tag{46}$$

$$\sum_{k=2}^{\infty} X_k P_1 P_k = \sum_{k=1}^{\infty} \frac{k+1}{2k+3} X_{k+1} P_k + \sum_{k=3}^{\infty} \frac{k}{2k-1} X_{k-1} P_k, \tag{47}$$

$$\sum_{k=2}^{\infty} X_k \frac{\mathrm{d}P_1}{\mathrm{d}\theta}\frac{\mathrm{d}P_k}{\mathrm{d}\theta} = \sum_{k=1}^{\infty} \frac{(k+1)(k+2)}{2k+3} X_{k+1} P_k - \sum_{k=3}^{\infty} \frac{k(k-1)}{2k-1} X_{k-1} P_k, \tag{48}$$

$$\begin{aligned}\sum_{k=2}^{\infty} X_k P_1^2 P_k = {} & \sum_{k=0}^{\infty} \frac{(k+1)(k+2)}{(2k+3)(2k+5)} X_{k+2} P_k + \sum_{k=2}^{\infty} \frac{2k^2+2k-1}{(2k-1)(2k+3)} X_k P_k \\ & + \sum_{k=4}^{\infty} \frac{k(k-1)}{(2k-3)(2k-1)} X_{k-2} P_k,\end{aligned} \tag{49}$$

$$\sum_{k=2}^{\infty} X_k P_k \left(\frac{\mathrm{d}P_1}{\mathrm{d}\theta}\right)^2 = \sum_{k=2}^{\infty} X_k P_k (1-P_1^2), \tag{50}$$

$$\begin{aligned}\sum_{k=2}^{\infty} X_k P_1 \frac{\mathrm{d}P_1}{\mathrm{d}\theta}\frac{\mathrm{d}P_k}{\mathrm{d}\theta} = {} & \sum_{k=0}^{\infty} \frac{(k+1)(k+2)(k+3)}{(2k+3)(2k+5)} X_{k+2} P_k + \sum_{k=2}^{\infty} \frac{k(k+1)}{(2k-1)(2k+3)} X_k P_k, \\ & - \sum_{k=4}^{\infty} \frac{k(k-1)(k-2)}{(2k-3)(2k-1)} X_{k-2} P_k.\end{aligned} \tag{51}$$

Electric contributions to normal-stress balance

Here we determine the electrostatic contribution to the normal-stress balance at S, given by Eq. 9. The normal component of the Maxwell stress, given by (12), exerted by the electric field on the bubble is

$$\begin{aligned}\hat{\mathbf{n}}\cdot(\hat{\mathbf{n}}\cdot\mathbf{M}) &= \overline{\varepsilon}\left[(\mathbf{E}\cdot\hat{\mathbf{n}})^2-\frac{1}{2}\mathbf{E}\cdot\mathbf{E}\right]\\ &= \overline{\varepsilon}\left\{\frac{1}{2}\left[\left(\frac{\partial\psi}{\partial r}\right)^2-\frac{1}{r^2}\left(\frac{\partial\psi}{\partial\theta}\right)^2\right]-\epsilon\frac{2}{r^2}\frac{\partial\psi}{\partial r}\frac{\partial\psi}{\partial\theta}\sum_{k=2}^{\infty}a_k\frac{\mathrm{d}P_k}{\mathrm{d}\theta}\right\},\end{aligned} \tag{52}$$

evaluated on S. For the liquid side of the interface

$$\begin{aligned}\hat{\mathbf{n}}\cdot(\hat{\mathbf{n}}\cdot\mathbf{M}) &= \overline{\varepsilon}\,\overline{\varepsilon}_0\left\{\frac{1}{2}(E_0-2A)^2P_1^2-\frac{1}{2}(E_0+A)^2\left(\frac{\mathrm{d}P_1}{\mathrm{d}\theta}\right)^2\right.\\ &\quad+\epsilon\sum_{k=2}^{\infty}\left[\frac{6A}{R}(E_0-2A)a_kP_1^2P_k-\frac{k+1}{R^{k+2}}(E_0-2A)A_kP_1P_k+\frac{3A}{R}a_k(E_0+A)P_k\left(\frac{\mathrm{d}P_1}{\mathrm{d}\theta}\right)^2\right.\\ &\quad\left.\left.-\frac{A_k}{R^{k+2}}(E_0+A)\frac{\mathrm{d}P_1}{\mathrm{d}\theta}\frac{\mathrm{d}P_k}{\mathrm{d}\theta}-\frac{2}{R}(E_0-2A)(E_0+A)a_kP_1\frac{\mathrm{d}P_1}{\mathrm{d}\theta}\frac{\mathrm{d}P_k}{\mathrm{d}\theta}\right]\right\}\\ &= P_0\overline{\varepsilon}\,\overline{\varepsilon}_0\left\{\frac{1}{6}\left(2A^2-8E_0A-E_0^2\right)-\epsilon\frac{2a_2}{5R}(A-2E_0)(A-E_0)\right\}\\ &\quad+P_1\overline{\varepsilon}\,\overline{\varepsilon}_0\left\{\epsilon\frac{6a_3}{35R}\left(A^2+11AE_0-8E_0^2\right)-\epsilon(2E_0-A)\frac{6A_2}{5R^4}\right\}\\ &\quad+P_2\overline{\varepsilon}\,\overline{\varepsilon}_0\left\{\frac{1}{3}\left(5A^2-2AE_0+2E_0^2\right)+\epsilon(A-2E_0)\frac{12A_3}{7R^5}+\epsilon\frac{4a_4}{21R}\left(5A^2+13AE_0-10E_0^2\right)\right.\\ &\quad\left.+\epsilon\frac{2a_2}{7R}\left(-13A^2+18AE_0-2E_0^2\right)\right\}\\ &\quad+\epsilon\overline{\varepsilon}\,\overline{\varepsilon}_0\sum_{k=3}^{\infty}P_k\left\{(A-2E_0)\frac{(k+1)(k+2)}{(2k+3)R^{k+3}}A_{k+1}+[A(3k-1)-E_0]\frac{kA_{k-1}}{(2k-1)R^{k+1}}\right.\\ &\quad+\left[A^2(4k-3)+AE_0(9+2k)-E_0^2(6+2k)\right]\frac{(k+1)(k+2)}{(2k+3)(2k+5)}\frac{a_{k+2}}{R}\\ &\quad+\left[A^2(-7k^2-7k+3)+AE_0(10k^2+10k-6)-E_0^2k(k+1)\right]\frac{2}{(2k-1)(2k+3)}\frac{a_k}{R}\\ &\quad\left.+(1-\delta_{3k})\left[-(4k+7)A^2+(7-2k)AE_0+2(k-2)E_0^2\right]\frac{k(k-1)}{(2k-3)(2k-1)}\frac{a_{k-2}}{R}\right\}.\end{aligned} \tag{53}$$

The corresponding contribution from the gas side is

$$\begin{aligned}\hat{\mathbf{n}}\cdot(\hat{\mathbf{n}}\cdot\mathbf{M}) &= -\overline{\varepsilon}_{\mathrm{in}}\overline{\varepsilon}_0\left\{-\frac{1}{2}B^2P_1^2+\frac{1}{2}B^2\left(\frac{\mathrm{d}P_1}{\mathrm{d}\theta}\right)^2+\epsilon\sum_{k=2}^{\infty}\left[-BB_kkR^{k-1}P_1P_k+BB_kR^{k-1}\frac{\mathrm{d}P_1}{\mathrm{d}\theta}\frac{\mathrm{d}P_k}{\mathrm{d}\theta}\right.\right.\\ &\quad\left.\left.+\frac{2B^2}{R}a_kP_1\frac{\mathrm{d}P_1}{\mathrm{d}\theta}\frac{\mathrm{d}P_k}{\mathrm{d}\theta}\right]\right\}+O(\epsilon^2)\end{aligned}$$

$$
\begin{aligned}
&= -\overline{\varepsilon}_{\text{in}}\overline{\varepsilon}_0 P_0\left\{\frac{1}{6}B^2+\epsilon\frac{4B^2}{5R}a_2\right\}-\overline{\varepsilon}_{\text{in}}\overline{\varepsilon}_0 P_1\left\{\epsilon\frac{2R}{5}BB_2+\epsilon\frac{48B^2}{35R}a_3\right\}\\
&\quad-\overline{\varepsilon}_{\text{in}}\overline{\varepsilon}_0 P_2\left\{-\frac{2}{3}B^2+\epsilon\frac{3R^2}{7}BB_3+\epsilon\frac{40B^2}{21R}a_4+\epsilon\frac{4B^2}{7R}a_2\right\}\\
&\quad-\overline{\varepsilon}_{\text{in}}\overline{\varepsilon}_0\epsilon\sum_{k=3}^{\infty}P_k\left\{\frac{(k+1)}{2k+3}BB_{k+1}R^k-\frac{2k(k-1)}{2k-1}BB_{k-1}R^{k-2}\right.\\
&\quad+\frac{2B^2}{R}\frac{(k+1)(k+2)(k+3)}{(2k+3)(2k+5)}a_{k+2}+\frac{2B^2}{R}\frac{k(k+1)}{(2k-1)(2k+3)}a_k\\
&\quad\left.-\frac{2B^2}{R}(1-\delta_{3k})\frac{k(k-1)(k-2)}{(2k-3)(2k-1)}a_{k-2}\right\}+O(\epsilon^2)\\
&= -\overline{\varepsilon}_{\text{in}}\overline{\varepsilon}_0 P_0\left\{\frac{1}{6}(E_0+A)^2+\epsilon(E_0+A)(2E_0+A)\frac{2a_2}{5R}\right\}\\
&\quad-\overline{\varepsilon}_{\text{in}}\overline{\varepsilon}_0 P_1\left\{\epsilon\frac{2A_2}{5R^4}(E_0+A)+\epsilon(E_0+A)\frac{6a_3}{35R}(8E_0+5A)\right\}\\
&\quad-\overline{\varepsilon}_{\text{in}}\overline{\varepsilon}_0 P_2\left\{-\frac{2}{3}(E_0+A)^2+\epsilon(E_0+A)\frac{a_2}{R}\left(\frac{7}{5}A+\frac{4}{7}E_0\right)+\epsilon\frac{4a_4}{21R}(E_0+A)(10E_0+7A)\right.\\
&\quad\left.+\epsilon\frac{3A_3}{7R^5}(E_0+A)\right\}-\overline{\varepsilon}_{\text{in}}\overline{\varepsilon}_0\epsilon\sum_{k=3}^{\infty}P_k(E_0+A)\left\{\frac{(k+1)A_{k+1}}{(2k+3)R^{k+3}}-\frac{2k(k-1)A_{k-1}}{(2k-1)R^{k+1}}\right.\\
&\quad+\frac{(k+1)(k+2)a_{k+2}}{(2k+3)(2k+5)R}\left[A(2k+3)+2E_0(k+3)\right]\\
&\quad+\frac{a_k}{R}\left[\frac{2E_0k(k+1)}{(2k-1)(2k+3)}+\frac{A(k-1)(3k+1)}{2k+1}\right]\\
&\quad\left.+(1-\delta_{3k})\frac{k(k-1)a_{k-2}}{(2k-1)(2k-3)R}\left[2A(2k-1)-2E_0(k-2)\right]\right\}
\end{aligned}
\tag{54}
$$

References

1. Dong W, Li RY, Yu HL, Yan YY (2006) An investigation of behaviours of a single bubble in a uniform electric field. Exp Therm Fluid Sci 30:579–586
2. Di Marco P, Grassi W, Memoli G, Takamasa T (2003) Influence of electric field on single gas-bubble growth and detachment in microgravity. Int J Multiph Flow 29:559–578
3. Spelt PDM, Matar OK (2006) The collapse of a bubble in an electric field. Phys Rev E 74:art. no. 046309
4. Lee SM, Kang IS (1999) Three-dimensional analysis of steady-state shape and small-amplitude oscillation of a bubble uniform and non-uniform electric fields. J Fluid Mech 384:59–91
5. Oh JM, Kim PJ, Kang IS (2001) Chaotic oscillation of a bubble in a weakly viscous dielectric fluid under electric fields. Phys Fluids 13:2820–2830
6. Tsamopoulos JA, Brown RA (1984) Resonant oscillations of inviscid charged drops. J Fluid Mech 147:373–395
7. Tsamopoulos JA, Akylas TR, Brown RA (1985) Dynamics of charged drop break-up. Proc R Soc Lond A 401:67–88
8. Feng JQ (1990) A method of multiple-parameter perturbations with an application to drop oscillations in an electric field. Q Appl Maths 48:555–567
9. Feng JQ, Beard KV (1990) Small-amplitude oscillations of electrostatically levitated drops. Proc R Soc Lond A 430:133–150
10. Feng JQ, Beard KV (1991) Resonances of a conducting drop in an alternating electric field. J Fluid Mech 222:417–435
11. Feng JQ, Beard KV (1991) Three-dimensional oscillation characteristics of electrostatically deformed drops. J Fluid Mech 227:429–447
12. Feng IS (1993) Dynamics of a conducting drop in a time-periodic electric field. J Fluid Mech 257:229–264
13. Feng ZC (1997) Instability caused by the coupling between non-resonant shape oscillation modes of a charged conducting drop. J Fluid Mech 333:1–21
14. Zharov AN, Shiryaeva SO, Grigor'ev AI (2003) On nonlinear vibrations of a charged drop in the third-order approximation in the amplitude of initial single-mode excitation. Tech Phys 48:697–707

15. Zharov AN, Shiryaeva SO, Grigor'ev AI (2003) Nonlinear vibration of a charged drop in a third-order approximation in the amplitude of multimode initial deformation. Tech Phys 48:1511–1521
16. Shiryaeva SO, Zharov AN, Grigor'ev AI (2004) On nonlinear resonant four-mode interaction between capillary vibrations of a charged drop. Tech Phys 49:8–18
17. Zharov AN, Grigor'ev AI (2003) On time evolution of the surface shape of a charged viscous liquid drop deformed at zero time. Tech Phys 50:19–29
18. Xu X, Homsy GM (2006) The settling velocity and shape distortion of drops in a uniform electric field. J Fluid Mech 564:395–414
19. Sherwood JD (1988) Breakup of fluid droplets in electric and magnetic fields. J Fluid Mech 188:133–146
20. Saville DA (1997) Electrohydrodynamics: the Taylor-Melcher leaky dielectric model. Annu Rev Fluid Mech 29:27–64
21. Belonozhko DF, Grigor'ev AI (2004) On the correct writing of the law of conservation of amount of substance at the moving fluid-fluid interface. Tech Phys 49:1415–1421
22. Stone HA (1990) A simple derivation of the time-dependent convective-diffusion equation for surfactant transport along a deforming interface. Phys Fluids A 2:111–112
23. Wong H, Rumschitzki D, Maldarelli C (1996) On the surfactant mass balance at a deforming fluid interface. Phys Fluids 8:3203–3204
24. Pereira A, Trevelyan PMJ, Thiele U, Kalliadasis S (2007) Dynamics of a horizontal thin liquid film in the presence of reactive surfactants. Phys Fluids 19:112102
25. Doinikov AA (2004) Translational motion of a bubble undergoing shape oscillations. J Fluid Mech 501:1–24
26. Prosperetti A, Lezzi A (1986) Bubble dynamics in a compressible liquid. Part I. First-order theory. J Fluid Mech 168:457–478
27. Lezzi A, Prosperetti A (1986) Bubble dynamics in a compressible liquid. Part II. Second-order theory. J Fluid Mech 185:289–321
28. Kang IS, Leal LG (1988) Small-amplitude perturbations of shape for a nearly spherical bubble in an inviscid straining flow (steady shapes and oscillatory motion). J Fluid Mech 187:231–266
29. Prosperetti A (1977) Viscous effects on perturbed spherical flows. Q Appl Mech 34:339–352
30. Prosperetti A, Seminara G (1978) Linear stability of a growing or collapsing bubble in a slightly viscous liquid. Phys Fluids 21:1465–1470
31. Brenner MP, Hilgenfeldt S, Lohse D (2002) Single-bubble sonoluminescence. Rev Mod Phys 74:425–484
32. Poritsky M (1951) The collapse or growth of a spherical bubble or cavity in a viscous fluid. In: Proceedings of the 1st U.S. congress of applied mechanics, Illinois Institute of Technology, pp 813–821
33. Wu CC, Roberts PH (1998) Bubble shape instability and sonoluminescence. Phys Lett A 250:131–136
34. Lamb H (1895) Hydrodynamics. Cambridge University Press, Cambridge
35. Basaran OA (1992) Nonlinear oscillations of viscous liquid drops. J Fluid Mech 241:169–198
36. McDougald NK, Leal LG (1999) Numerical study of the oscillations of a non-spherical bubble in an inviscid, incompressible liquid. Part I. Free oscillations from non-equilibrium initial conditions. Int J Multiph Flow 25:887–919
37. Shaw SJ (2006) Translation and oscillation of a bubble under axisymmetric deformation. Phys Fluids 18:art. no. 072104
38. Benjamin TB, Ellis AT (1990) Self-propulsion of axisymmetrically vibrating bubbles. J Fluid Mech 212:65–80
39. Feng ZC, Leal LG (1995) Translational instability of a bubble undergoing shape oscillations. Phys Fluids 7:1325–1336
40. Kushch VI, Sangani AS, Spelt PDM, Koch DL (2002) Finite Weber number motion of bubbles through a nearly inviscid liquid. J Fluid Mech 460:241–280